Enhancement and control of a coherent localized surface plasmon through pump-pulse engineering

Ankit Purohit [1,*] and Akhilesh Kumar Mishra [1,2,†]

[1]*Department of Physics, Indian Institute of Technology Roorkee, Roorkee-247667, Uttarakhand, India*

[2]*Centre for Photonics and Quantum Communication Technology, Indian Institute of Technology Roorkee, Roorkee- 247667, Uttarakhand, India*

(Received 15 January 2024; accepted 14 May 2024; published 4 June 2024)

This article investigates a spaser geometry in which a silver nanoparticle is enclosed by Λ-type three-level gain media in the form of quantum dots. An intense Gaussian pump pulse induces population transfer in this Λ-type quantum dot gain medium. The transition energy from the gain medium is transferred to the nearby localized surface-plasmon (LSP) mode of the silver nanoparticle, resulting in a highly intense and coherent generation of LSPs. We demonstrate that an optimum value of pump-pulse width and pulse amplitude is required for an intense and coherent LSP generation. A Gaussian pump pulse can lead to Gaussian-shape temporal and spectral LSP profiles. However, as the pump pulse broadens, the Gaussian-shape LSP profile gets distorted, resulting in less intense and asymmetric temporal as well as spectral profiles. In practice, detuning typically exists between the pump frequency and the transition frequency of the quantum dot energy levels. Consequently, employing adiabatic rapid passage phenomena through a linearly chirped Gaussian pulse emerges as an effective technique for ensuring robust population transfer within the energy levels of the quantum dots. This further enhances the number of LSPs. Furthermore, the study addresses the effect of detuning noise in the output of the spaser system. Thus, a shaped pump pulse also enables manipulation of the temporal and spectral profiles of LSPs.

DOI: 10.1103/PhysRevA.109.063505

I. INTRODUCTION

Nanophotonics and quantum optics have witnessed remarkable developments in recent years that introduced innovative ways of manipulating light and matter at the nanoscale [1–5]. Among the myriad of emerging technologies, plasmon-based optical components have garnered significant attention for their potential to integrate with electronic counterparts, enabling a new era of efficient and compact nanoscale devices [6–8]. This integration is made possible by the intriguing phenomenon of localized surface plasmons (LSPs), where light can be confined and manipulated within nanosized metal structures [9]. The integration of the optoelectronic devices warrants an understanding of the fundamental coupling mechanism between different optical systems at the nanoscale. To this end, the concept of plasmon and quantum emitter coupling has been studied rigorously in literature [10,11].

Surface-plasmon amplification by stimulated emission of radiation (spaser), often known as nanolaser, has attracted a considerable amount of research attention during the past two decades [12–15]. In 2003, Bergman and Stockman proposed the idea of spaser, which is the amplification of a coherent LSP mode on the nanosize metal structure [16,17]. When light is incident on the gain medium, excitons (electron-hole pairs) are formed, which upon relaxation to their initial state release their transition energy in the form of photons. Since, in the geometry under consideration, the metal nanoparticles supporting LSP are placed very close to the emitter, this energy is directly transferred to the plasmon mode. Continuous pumping to gain medium and feedback from LSP result in an amplified coherent LSP. The main advantage of a LSP is localization of the electromagnetic field in space as well as in time. Spasers harness the principles of both lasers and surface-plasmon resonances to achieve coherent emission of light of subwavelength volumes, holding the potential to revolutionize applications in nanophotonics, sensing, and optoelectronics domains. Later, surface-plasmon polariton mode lasers have been suggested and demonstrated successfully [15]. Subsequently, several types of nanolasers have been proposed such as plasmon nanowire laser, nanopatch laser, nanodisk laser, metal-coated nanolaser, and so on [18–21]. Merits and challenges with these nanolasers have also been detailed in recent literature [12]. The potential applications of these nanolasers are in optical interconnect, sensing, spectroscopy, optical probing of biological samples, and eigenmode engineering, among others [22–26]. Spaser performance can be engineered by controlling three basic components: pump source, gain medium, and plasmon cavity. An ample amount of literature is available on different kinds of plasmon cavities and their performance towards realizing efficient lasing [12,15]. Recently, we have shown that the continuous mode spaser performs well when the quantum dot (QD) gain medium is pumped incoherently [27]. In addition, the preparation of a gain medium sample is substantially important for an efficiently working spaser. For example, in the presence of linear electron-phonon interactions, the spaser spectrum shows a small peak at the

*a_purohit@ph.iitr.ac.in

†akhilesh.mishra@ph.iitr.ac.in

wings that owe its origin to the periodic time-harmonic solution of LSPs in steady state [28].

Since the transition energy of the gain medium is used to amplify the coherent plasmon mode, it is necessary to have precise control of the population transfer in the gain medium. Practically, there always exists some detuning between the pump-pulse frequency and the transition frequency of the gain medium. This detuning constrains the population transfer in the upper energy level. In the early days, the π pulse method (where the integrated area of the Rabi frequency is equal to π) was used for complete population transfer but this method is very sensitive to the resonance frequency, amplitude, and the temporal profile of pulse [29,30]. Adiabatic rapid passage (ARP) has long been suggested to encounter the problem of incomplete population transfer in two- or many-level systems. The phenomenon of ARP is robust against the detuning factor and coupling variation [31–34]. In this phenomenon, a linear chirp is introduced in the pulse that sweeps through the transition frequency of two energy-level quantum systems. Depending on the sign of the chirp parameter, the frequency is swept either above or below the transition frequency and a robust population transfer is achieved [31]. For an efficient transfer of population through ARP, the frequency sweep must be fast compared to the excited state lifetime and slow compared to the resonant Rabi frequency. Depending on the numerical sign of the chirp, linear chirp may have two types: up chirp (or positive chirp) and down chirp (negative chirp). In up chirp, the instantaneous frequency increases linearly from leading to trailing edge while in down chirp the opposite occurs [35,36]. The optimal transfer of population is achieved by sweeping the pump frequency through resonance. It has been demonstrated experimentally that efficient frequency swept by the chirped pulse results in robust population transfer in quantum emitters [32–34,37,38].

Like traditional lasers, spasers are susceptible to various noise sources, including spontaneous emission, thermal fluctuations, and electronic noise. Noise can profoundly impact the efficiency and coherence of spaser emissions, a crucial consideration for practical applications. Noise can take various forms, two of which are "off-diagonal noise," associated with variations in coupling strength between energy levels, and "diagonal noise," linked to alterations in energy-level spacing. Several forms of off-diagonal noise have been investigated in the literature, such as Gaussian noise, harmonic noise, and slow off-diagonal noise [39]. The robustness against noise is crucial for assessing the device's quality. Usually, the high-frequency noise does not impact observability (i.e., number of LSPs) because it is highly detuned from the plasmon frequency or the transition frequency of the gain medium. In the present work, we have considered the noise arising from the time-harmonic fluctuation of detuning between pump-pulse frequency and transition frequency.

The Λ-type semiconductor QDs have extensively been explored for coherent population trapping used to explore "laser without inversion" or electromagnetically induced transparency phenomena [1,40–42]. The Λ-type system is a well-known three-level system, which is routinely used for semiconductor QDs [14,40–44]. Such three-level systems are achieved by employing either the external magnetic field or the external voltage source on a two-level system of QDs [40,41]. These III-V QDs have been used as a gain medium for lasers and spasers [42–45].

In this article, we merge the concept of ARP with the plasmon laser. We show that an optimum pulse width is required for an efficient population transfer in the gain medium. Since the population transfers couples to the plasmon mode, the number of LSPs increases accordingly. The population transfer is further enhanced by using the chirp Gaussian pump pulse in place of the transform-limited one. Depending on the pulse width, an optimized chirp is required for robust population transfer. This study also reveals that pulses of larger power may boost the population transfer between the energy levels involved but this does not always help in increasing the number of LSPs. In particular, we show the variation in number of LSPs with the pump-pulse parameter and provide an optimized pulse parameter to observe the larger number of LSPs. Nonetheless, the ARP technique has been used to counter the time-harmonic fluctuation of detuning and coupling factors so that the intense LSP is observed.

This article is arranged as follows: In Sec. II, the spaser model and mathematical equations are presented. In Sec. III, we present the temporal and spectral profiles of LSPs. In this section, the pump-pulse parameters (pulse width and amplitude) are optimized in such a way that a large number of LSPs are generated. In this section, we also show that a linearly chirped pulse helps encounter the time-harmonic noise. Section IV summarizes the work.

II. MODEL AND EQUATIONS

In the considered spaser geometry, as shown schematically in Fig. 1(a), a metal nanoparticle is surrounded by a large number of similar QDs. These QDs are a three-level Λ system, which is a typical energy-level arrangement in semiconductor QDs such as GaAs or CdSe QDs [14]. A Gaussian pulse is used to pump the population from QD level $|2\rangle$ to QD level $|3\rangle$. The population from level $|3\rangle$ decays to level $|2\rangle$ and level $|1\rangle$ with decay rates γ_{32} and γ_{31}, respectively. The nonradiative transition from level $|3\rangle$ to level $|1\rangle$ couples to the LSP mode of metal nanoparticles [see Fig. 1(b)]. As a result, a large number of coherent LSPs are generated. The transition from energy level $|2\rangle$ to energy level $|1\rangle$ is dipole forbidden due to selection rules [40,41]. We would like to note here that energy levels $|2\rangle$ and $|1\rangle$ are the Zeeman-split ground state energy levels and level $|3\rangle$ is exciton level [40,41].

The total Hamiltonian for the above system in rotating wave approximation is expressed as

$$H = \hbar\omega_n \hat{a}_n^\dagger \hat{a}_n + \sum_p \left[\sum_{i=1,2,3} \hbar\omega_i^p |\mathrm{i}\rangle\langle \mathrm{i}| + \hbar\left(\Omega_c^p |3\rangle\langle 2| + \Omega_b^p |3\rangle\langle 1| + \mathrm{c.c.}\right)\right]. \tag{1}$$

The number of QDs surrounding the metal nanoparticle is $\sum_p = N_p$. Since all the QDs couple equivalently with the LSP mode, it is suitable to omit the index p. The Rabi frequency for $|3\rangle \rightarrow |2\rangle$ transition is written as $\Omega_c = d_{32}E(t)/\hbar = \Omega_0 \exp(-i\omega_c t)\exp[-(1+iC)t^2/2\tau^2]$, where d_{32}

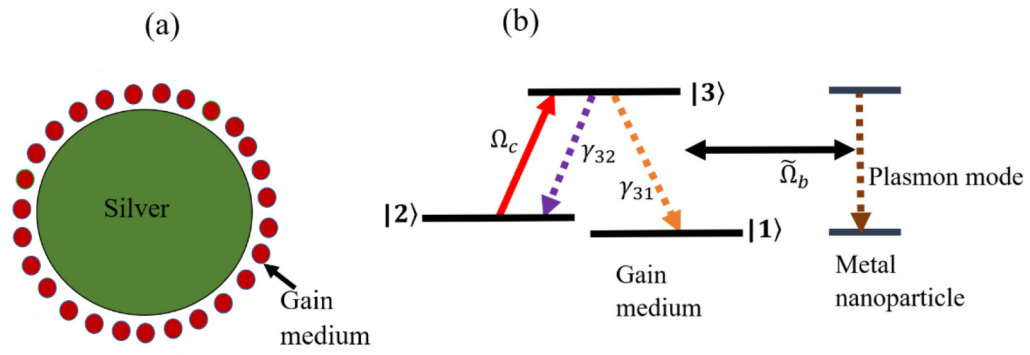

FIG. 1. (a) Schematic of spaser geometry, where a metal nanoparticle is surrounded by large number of QDs. (b) Energy-level diagram of three-level Λ-type QDs and dipolar plasmon mode.

is the transition dipole moment of $|3\rangle$ to $|2\rangle$ level, $E(t) = A\ \exp(-i\omega_c t)\exp[-(1+iC)t^2/2\tau^2]$ is the chirp Gaussian pump pulse, where C is chirp parameter, ω_c is pump frequency, A is pulse amplitude, and τ is pulse width. The Rabi frequency for the $|3\rangle \rightarrow |1\rangle$ transition is given by $\Omega_b = d_{31}E_b(t)/\hbar = \tilde{\Omega}_b\hat{a}_n(t)$, where d_{31} is the transition dipole moment of $|3\rangle$ to $|1\rangle$ level, $\tilde{\Omega}_b$ is the single plasmon Rabi frequency, *and* $\hat{a}_n$ is the LSP annihilation operator [9,14,27].

The density matrix elements for QDs is defined by a von Neumann equation, which is given as

$$\dot{\hat{\rho}} = -\frac{i}{\hbar}[H, \hat{\rho}] + L(\hat{\rho}), \tag{2}$$

where the Lindblad operator, L, accounts for the dissipation rate of QDs and LSPs and is given by

$$\begin{aligned} L(\hat{\rho}) = &\frac{\gamma_{32}}{2}(2\sigma_k\hat{\rho}\sigma_k^\dagger - \sigma_k^\dagger\sigma_k\hat{\rho} - \hat{\rho}\sigma_k^\dagger\sigma_k) \\ &+ \frac{\gamma_{31}}{2}(2\sigma_m\hat{\rho}\sigma_m^\dagger - \sigma_m^\dagger\sigma_m\hat{\rho} - \hat{\rho}\sigma_m^\dagger\sigma_m) \\ &+ \frac{\gamma_n}{2}(2\hat{a}_n\hat{\rho}\hat{a}_n^\dagger - \hat{a}_n^\dagger\hat{a}_n\hat{\rho} - \hat{\rho}\hat{a}_n^\dagger\hat{a}_n), \end{aligned} \tag{3}$$

where $\sigma_k = |2\rangle\langle 3|$ and $\sigma_m = |1\rangle\langle 3|$ are the transition operators for the three-level QDs, γ_{ij} is the spontaneous decay rate in respective $|i\rangle \rightarrow |j\rangle$ levels, and γ_n is the decay rate of the LSP.

To make the Hamiltonian time independent, the following transformations have been employed [2]:

$$\begin{aligned} &\hat{\rho}_{21} = \rho_{21}e^{-i\omega_{21}t}; \quad \hat{\rho}_{31} = \rho_{31}e^{-i\omega_0 t}; \\ &\hat{\rho}_{32} = \rho_{32}e^{-i\omega_c t} \quad \text{and} \quad \hat{a}_n = a_{0n}e^{-i\omega_0 t}, \end{aligned}$$

where $\rho_{31}, b_{0m}, \rho_{32}$, and a_{0n} are the slowly varying amplitudes. The frequency terms defined as $\omega_{21} = \omega_2 - \omega_1$, $\omega_{32} = \omega_3 - \omega_2$, and $\omega_{31} = \omega_3 - \omega_1$. The spasing transition frequency, ω_0, is defined as $\omega_0 = (\omega_{31}\gamma_{31} + \omega_n\gamma_n)/(\gamma_n + \gamma_{31})$ [9,27]. The number of LSPs is given by $N_n = |a_{0n}(t)|^2$.

The density matrix elements for any pth QD are given by

$$\dot{\rho}_{11} = \gamma_{31}\rho_{33} + i[\Omega_b\rho_{31}^* - \Omega_b^*\rho_{31}], \tag{4a}$$

$$\dot{\rho}_{22} = \gamma_{32}\rho_{33} + i[\Omega_c\rho_{32}^* - \Omega_c^*\rho_{32}], \tag{4b}$$

$$\dot{\rho}_{31} = -\left(\frac{\gamma_{31}+\gamma_{32}}{2}\right)\rho_{31} + i[\Omega_b(\rho_{33} - \rho_{11}) - \Omega_c\rho_{21}], \tag{4c}$$

$$\dot{\rho}_{21} = i[\Omega_b\rho_{23} - \Omega_c^*\rho_{31}], \tag{4d}$$

$$\dot{\rho}_{32} = i\Delta_c\rho_{32} - \left(\frac{\gamma_{31}+\gamma_{32}}{2}\right)\rho_{32} + i[\Omega_c(\rho_{33} - \rho_{22}) - \Omega_b\rho_{21}^*]. \tag{4e}$$

We define the detuning terms as $\Delta_c = \omega_c - \omega_{32}$. The density matrix elements satisfy the following conservation rule:

$$\rho_{11} + \rho_{22} + \rho_{33} = 1. \tag{5}$$

The temporal evolution for dipolar LSPs is given by

$$\dot{a}_{0n} = -\Gamma_n a_{0n} - i\sum_p \rho_{31}\tilde{\Omega}_b, \tag{6}$$

where $\Gamma_n = \gamma_n + i\Delta_n$, γ_n is the surface-plasmon relaxation rate, $\Delta_n = \omega_n - \omega_0$, and $\tilde{\Omega}_b = \Omega_b/a_{0n}$ is a single plasmon Rabi frequency.

III. RESULTS AND DISCUSSION

We solve the time evolution equations (4a)–(4e), (5), and (6) to study the dynamics of gain medium and LSPs. We require $\rho_{33} > \rho_{11}$ at initial time (i.e., $t = 0$) to amplify the LSP. When all the population is in level $|2\rangle$ [i.e., $\rho_{22}(0) = 1$] and other energy levels are empty [$\rho_{11}(0) = 0$, $\rho_{33}(0) = 0$], the LSP decays due to very high dissipation rate of metal ($\gamma_n \sim 10^{14}\ \text{s}^{-1}$) before the population reaches to level $|3$ and population inversion is achieved. As a result, no amplification of the LSP occurs. Therefore, for amplification of the LSP, the population inversion needs to be created before the LSP decays [9]. To delineate the effects of pump-pulse parameters on the temporal and spectral profiles of the spaser, even before pumping the system, we consider that a low-energy flash produces a population distribution in the QDs energy level such that at the initial time (i.e., $t = 0$) $\rho_{11}(0) = 0$, $\rho_{33}(0) = 0.05$, and $\rho_{22}(0) = 0.95$. A low pump source or external voltage can be employed to initialize the density matrix elements [37,38]. We would like to emphasize here that the system under investigation does not require a very particular initialization. The essential condition for observing the results of the article is that ρ_{33} must be greater than ρ_{11} (i.e., $\rho_{33} > \rho_{11}$) for a Λ-type gain system. Even a modest population in ρ_{33} is adequate to achieve a significant enhancement in the spaser [42]. For any Λ-type system, as long as ($\rho_{33} > \rho_{11}$), irrespective of the quantitative value of the initialization, the results of the article will be qualitatively the same. Equation

TABLE I. Numerical values of the simulation parameters of QDs and metal nanoparticle [14].

Parameter	Numerical value
γ_{32}	2.8×10^{11} s^{-1}
γ_{31}	4×10^{12} s^{-1}
γ_n	10^{14} s^{-1}
Δ_n	3×10^{12} s^{-1}
Δ_c	5×10^{12} s^{-1}
N_p	24.60×10^4
$\tilde{\Omega}_b$	2.24×10^{11} s^{-1}
Ω_0	8×10^{12}

(6) indicates that the time evolution of a_{0n} depends on the ρ_{31} and coupling parameter $\tilde{\Omega}_b$. On the other hand, Eq. (4c) reveals that the term having ρ_{31} can be controlled by the external pump parameter Ω_c. Unless specified otherwise, the following simulation parameters shown in Table I have been used in our simulations.

In the subsequent section, we focus on analyzing the temporal and spectral profiles of the spaser with the input pump-pulse parameters. We aim to obtain the optimum pulse parameter to observe the intense LSPs.

A. Optimum pump-pulse width for transform-limited Gaussian pulse

In the spaser system, the QDs are pumped by the Gaussian pulse, whose envelope is expressed as

$$E(t) = A\exp\left[-\left(\frac{(t-3.2\tau)^2}{2\tau^2}\right)\right], \tag{7}$$

where A is pulse amplitude and τ is pulse width. Note that the time (t) is deliberately delayed by a factor of 3.2 times the pulse width to ensure that the leading edge of each pulse commences from time $t = 0$ in the simulation. For the Gaussian envelope, the temporal profiles of $\Omega_c(t)$ for two different pulse widths $\tau = 0.09$ and 0.25 ps are plotted in Fig. 2.

The transform-limited Gaussian pump pulse couples the transition from level $|2\rangle$ to level $|3\rangle$ with a time-dependent strength $\Omega_c\,(t)$. In Fig. (3), the time evolutions of ρ_{11}, ρ_{22}, ρ_{33}, and N_n are presented. For the Λ-type gain medium, N_n starts to build up at a time when the time evolution of ρ_{11} intersects with ρ_{22}, as depicted in Figs. 3(a) and 3(c). These figures also depict that the threshold time occurs early for the narrow pulse widths. The peak of N_n is observed at a time when the time evolution of ρ_{33} intersects with that of ρ_{11} and beyond this point N_n starts to decay. For the narrow pulse width, N_n and its spectrum have Gaussian shapes, as shown in Figs. 3(c) and 3(d), respectively. However, as the pulse broadens, the oscillatory decay observed in ρ_{33}, as seen in Fig. 3(b), distorts the Gaussian nature of N_n and its spectrum as shown in Figs. 3(c) and 3(d), respectively. Figure 3(e) displays an image plot of the time evolution of N_n up to 0.4 ps pulse width. This figure illustrates that as the pulse width increases, the peak of N_n proportionally shifts in time. At a specific pulse width, approximately 0.09 ps in our case, an intense N_n is observed. The optimum pulse width is highly sensitive to the parameters of the gain medium, as specified in Table I. For the given set of parameters, a Gaussian shape, intense N_n is observed near 0.09 ps, as seen in the image plot of Fig. 3(e).

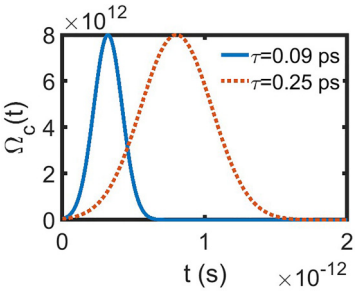

FIG. 2. Temporal profile of $\Omega_c(t)$ at $\Omega_0 = 8 \times 10^{12}$.

The spaser field is determined by taking the Fourier transform of $a_{0n}(t)$ [4,7], which is expressed as

$$E(\omega) = \int_0^T a_{0n}(t)\exp(i\omega t)dt. \tag{8}$$

For the broader pulses, as the peak of N_n shifts to the larger time, the spectrum shifts to the blue side. Figure 3(f) displays the spaser spectrum for the pulse width up to 0.4 ps. This analysis reveals that an asymmetric and non-Gaussian spectral profile is observed for the broader pulses.

B. Optimum chirp parameter

As mentioned in the Introduction, efficient population transfer in the upper level of QDs can be achieved using the chirped Gaussian pulse when there is detuning between the pump-pulse frequency and the transition frequency of QD energy levels. Equations (6) and (4c) demonstrate that the time evolution of N_n depends on the ρ_{33}. Hence, the time evolution of N_n can be manipulated by employing a chirped pump pulse. The chirped Gaussian pulse envelope can be expressed as

$$E(t) = A\exp\left[-\left(\frac{1+iC}{2\tau^2}\right)(t-3.2\tau)^2\right]. \tag{9}$$

For an unchirped Gaussian pulse ($C = 0$), the frequency bandwidth, $\Gamma = 1/\tau$. However, the bandwidth increases for the Gaussian chirp pulse, as shown by the following expression:

$$\Gamma' = \frac{1}{\tau}(1+C^2)^{1/2}, \tag{10}$$

where Γ' is the modified bandwidth of the Gaussian chirp pulse. Depending on the numerical sign of C, linear chirp may have two types: up chirp (positive C) and down chirp (negative C). The optimal transfer of population is achieved by sweeping the frequency through resonance. The instantaneous frequency of the linearly chirped Gaussian pulse is given by [35]

$$\omega(t) = \omega_c + C(t-3.2\tau)/\tau^2. \tag{11}$$

Now, the detuning parameter is defined as $\Delta_c(t) = \omega(t) - \omega_{32} = \omega_c - \omega_{32} + C(t-3.2\tau)/\tau^2 = \Delta_c + C(t-3.2\tau)/\tau^2$. Therefore, for the resonance [i.e., $\Delta_c(t) = 0$], chirp (C)

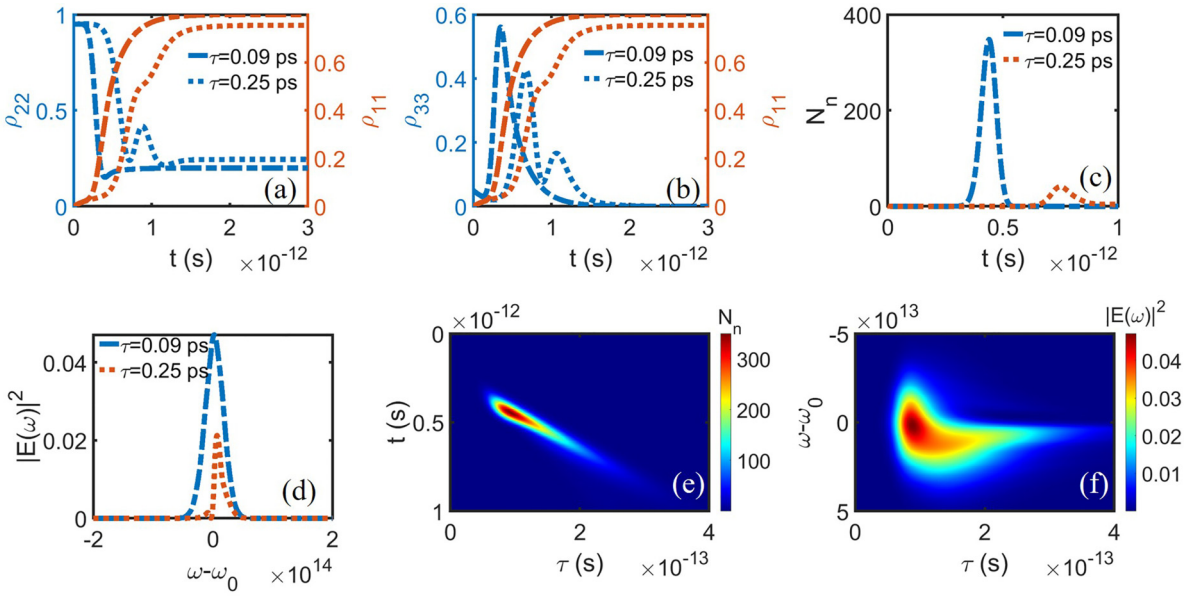

FIG. 3. Time evolution of (a) ρ_{22}, ρ_{11}, (b) ρ_{33}, ρ_{11}, (c) N_n, and (d) spaser spectrum ($|E(\omega)|^2$) when pumped by the Gaussian pulse having 0.09 and 0.25 ps pulse widths. (e) Image plots of N_n and spaser spectrum when the pulse width is varied up to 0.40 ps.

should be negative. So, in the case of detuning, the chirp parameter is helpful for the frequency matching, and this increases the population transfer in the upper level of the QD. The numerical sign of the detuning factor decides whether an up or down chirped pulse is required for the efficient population transfer. Note that the optimum chirp value depends on the pulse width. We would like to mention again that in the presence of a relaxation term, the requirement for ARP to occur is $\Omega_0\gamma_{32} \ll C/\tau^2 \ll \Omega_0^2$ [31,39,46].

Figure 4 displays the temporal evolutions of ρ_{11}, ρ_{22}, ρ_{33}, N_n and the spectral profile for the spaser under various chirp values. The population dynamics of ρ_{22}, ρ_{11}, and ρ_{33} for $\tau = 0.09$ ps are depicted in Figs. 4(a) and 4(b). In the case of negative chirp ($C = -0.5$), Fig. 4(a) demonstrates that the intersection between ρ_{22} and ρ_{11} occurs earlier for $C = -0.5$ as compared to $C = 0$. Hence, N_n starts to build up early and leads to a larger N_n. The peak of N_n coincides with the time at which ρ_{33} intersects with ρ_{11}. Figure 4(c) reveals that for a pulse of width $\tau = 0.09$ ps, N_n maximizes near $C = -0.5$ due to maximum population transfer from ρ_{22} to ρ_{33}. For a broader

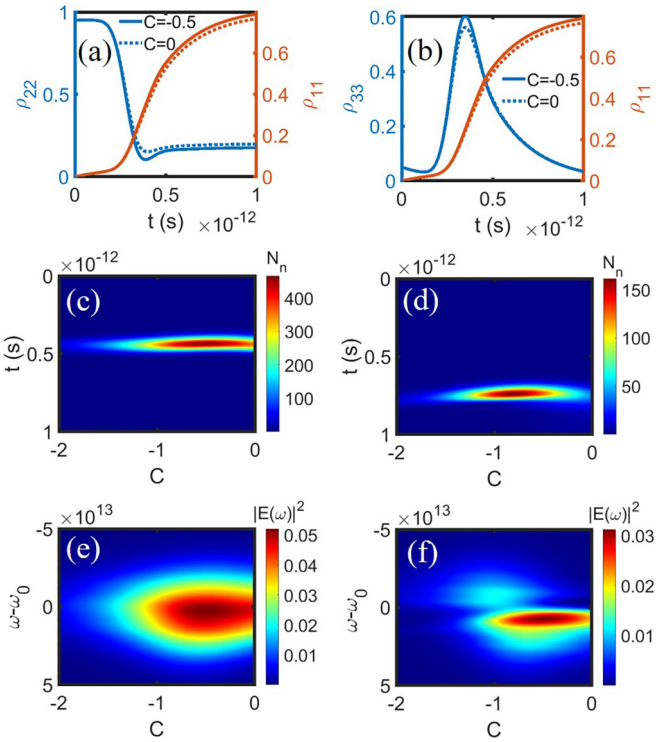

FIG. 4. Time evolutions of (a) ρ_{22}, ρ_{11}, (b) ρ_{33}, ρ_{11}, (c) temporal and (e) spectral profiles of LSP for different chirp values at $\tau = 0.09$ ps. (d) and (f) same as (c) and (e) but for $\tau = 0.25$ ps.

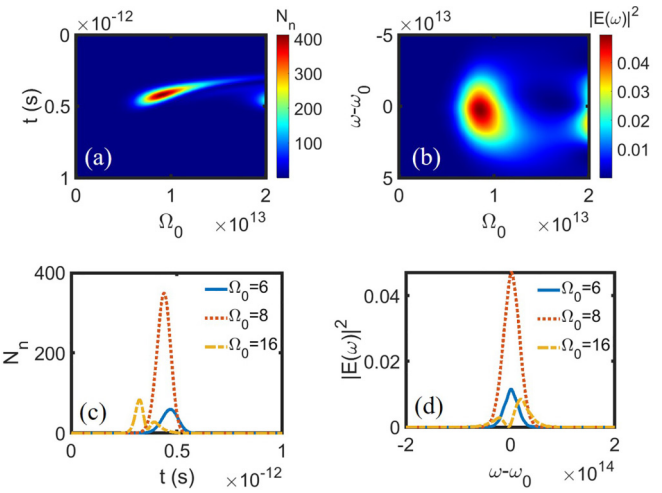

FIG. 5. Time evolution of N_n and corresponding spaser field at $C = 0$ for $\tau = 0.09$ ps, (a), (c) N_n and (b), (d) spaser spectrum. The value of Ω_0 in (c) and (d) is in 10^{12} s^{-1} order.

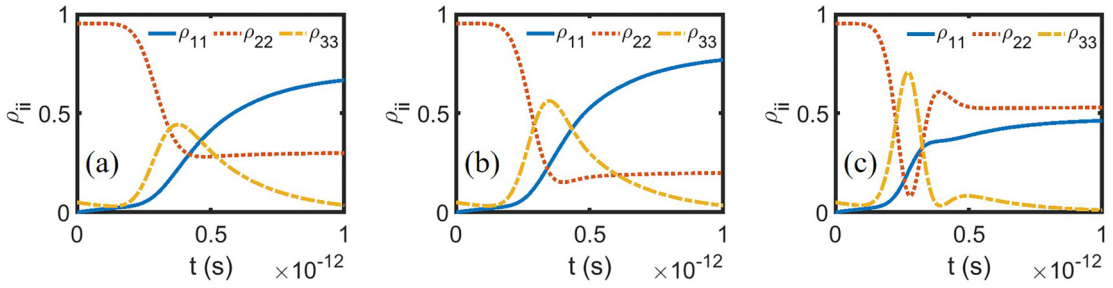

FIG. 6. Time evolution of ρ_{11}, ρ_{22}, and ρ_{33} for (a). $\Omega_0 = 6 \times 10^{12}$ s^{-1}, (b) $\Omega_0 = 8 \times 10^{12}$ s^{-1}, and (c) $\Omega_0 = 16 \times 10^{12}$ s^{-1}.

pump pulse, the value of the optimum chirp changes; for instance, for $\tau = 0.25$ ps the optimum chirp is $\sim C = -0.9$, as depicted in Fig. 4(d). Therefore, depending on the pulse width, the population in ρ_{33} maximizes for different optimum chirp values. At a very large negative chirp, there is high detuning between the pump-pulse frequency and the transition frequency of the QD, which leads to less population transfer in ρ_{33}. Consequently, N_n decreases. This analysis shows that an optimum chirp is required to obtain large N_n. It is worth noting that with a broader pump pulse, the population transfer in ρ_{33} takes a longer time, resulting in a time-shifted peak of N_n with smaller peak amplitude.

The spaser spectral profiles for $\tau = 0.09$ ps and $\tau = 0.25$ ps are shown in Figs. 4(e) and 4(f), respectively. For $\tau = 0.09$ ps, the Gaussian-like spectral profile of the spaser remains intact for all the considered chirp values. However, for $\tau = 0.25$ ps, as seen in Fig. 4(f), an asymmetric spectral distribution is observed. For larger negative chirp, the spaser spectrum becomes broader as depicted in Fig. 4(f). This shows that the input chirp plays an important role in manipulating the spaser spectrum.

C. Optimum pulse amplitude [or Rabi constant (Ω_0)]

Increasing the amplitude of the pump pulse does not always ensure an increase in the peak value of N_n, as displayed in Fig. 5(a). Figure 5(a) shows the evolution of N_n with Ω_0. It is observed that for a specific value of Ω_0 ($\sim 8 \times 10^{12}$), the time variation of N_n shows an intense Gaussian shape for a pump-pulse width $\tau = 0.09$ ps. However, as the Ω_0 varied, the Gaussian shape of N_n is distorted dramatically and its intensity reduces considerably. For a fixed pulse width ($\tau = 0.09$ ps), the peak of N_n is shifts in time with Ω_0, ultimately altering the corresponding spaser spectrum also [see Fig. 5(b)].

In the case of chirped pump-pulse excitation, for a fixed pulse width, although the numerical value of N_n changes its shape remains preserved. Figures 5(c) and 5(d) depict the temporal evolution of N_n and the spaser spectrum, respectively, for three different values of Ω_0. These figures emphasize the importance of selecting the optimal Ω_0 to attain a substantial N_n. Importantly, as discussed previously, as the pulse width deviates from an optimum value, a non-Gaussian-shaped N_n is observed. Hence, achieving a Gaussian-shaped and intense N_n necessitates the selection of an optimal combination of τ and Ω_0.

For a given pulse width, an increase in Ω_0 increases the pulse area, leading to more population transfer in ρ_{33}, which should enhance N_n. However, this does not happen because the temporal shape and intensity of N_n depend not only on the energy-level population of the gain medium, but more importantly on the temporal dynamics, as shown in Figs. 5 and 6. As pointed out earlier, the number of LSPs starts to accumulate at a time point when ρ_{22} intersects with ρ_{11} and the peak of N_n occurs when ρ_{33} coincides with ρ_{11}. The shape of N_n is intricately linked to the relative temporal dynamics of ρ_{11}, ρ_{22}, and ρ_{33}. For larger Ω_0, the time evolution of the density matrix elements intersect with each other in a complicated manner, as shown in Fig. 6(c); this results in the non-Gaussian shape of N_n. Therefore, a larger value of Ω_0 does enhance the population transfer in ρ_{33} but that does not guarantee an intense N_n.

D. Effect of time-harmonic detuning term [$\Delta_c(t)$] on N_n

In this section, we address the effects of noise on N_n due to time-dependent detuning. In particular, we consider harmonic time-dependent noise in detuning. In the presence of such noise, the time-dependent detuning term is expressed as $\Delta_c(t) = \delta \cos(\omega_p t)$, where δ is the amplitude of noise and

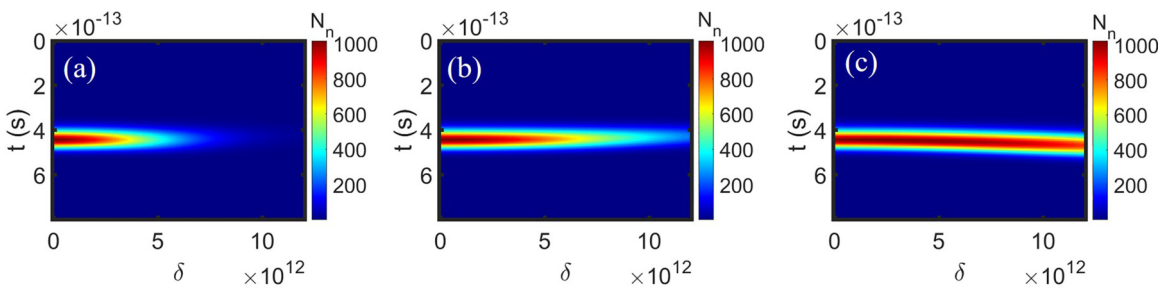

FIG. 7. Temporal profile of N_n for (a) $\omega_p = 0.2\Omega_0$, (b) $\omega_p = \Omega_0$, and (c) $\omega_p = 2\Omega_0$.

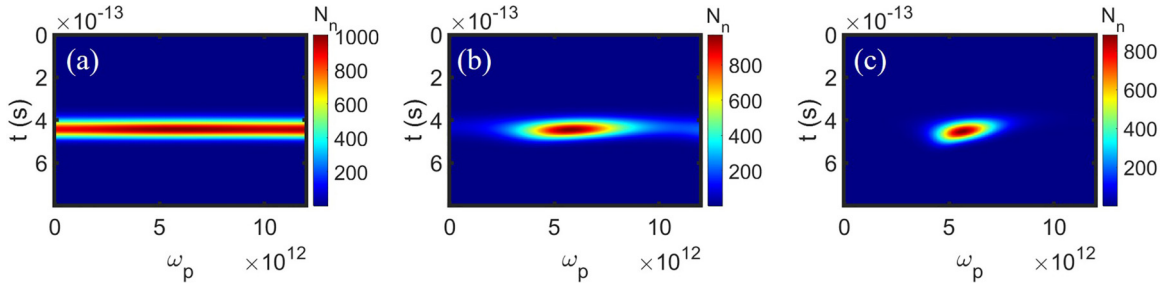

FIG. 8. Temporal profile of N_n for (a) $\delta = 0.2\Omega_0$, (b) $\delta = \Omega_0$, and (c) $\delta = 2\Omega_0$.

ω_p is the frequency thereof. This time-fluctuating detuning factor corresponds either to a change in the energy level of the gain medium or the pump-pulse frequency. The simulation parameters used in this section are the same as those of Table I except for the pump-pulse width, which here is $\tau = 0.09$ ps.

Figure 7 displays the time evolution of N_n for $\omega_p = 0.2\Omega_0$, , Ω_0, and $2\Omega_0$. When $\omega_p \ll \Omega_0$, a substantial reduction in the number of LSPs for larger δ are observed, as depicted in Fig. 7(a). For $\omega_p = \Omega_0$, a sufficient value of N_n is observed even for larger values of δ as shown in Fig. 7(b). At significantly higher values of ω_p ($\omega_p = 2\Omega_0$), a solitary-like temporal evolution is observed in Fig. 7(c). This discussion underscores that the temporal profile of N_n crucially depends on the noise frequency, ω_p, and noise amplitude, δ. As mentioned earlier, at higher frequencies noise detunes with the spaser system. Hence higher frequencies do not influence the N_n considerably, and that is what we observe in Fig 7.

To further explore the influence of ω_p for different values of δ, the time evolution of N_n is observed with ω_p. When δ is significantly smaller than Ω_0 (i.e., $\delta = 0.2\Omega_0$), the coupling term dominates over the detuning term. As a result, a notable peak of N_n is observed for a range of ω_p values as compared to the time-independent detuning. This is displayed in the temporal evolution of the spaser for the $\delta = 0.2\Omega_0$ in Fig. 8(a).

On the other hand, there is a dramatic variation in N_n when detuning factor δ is comparable or larger than the coupling term Ω_0. Figures 8(b) and 8(c) depict the temporal profile of N_n for $\delta = \Omega_0$ and $2\Omega_0$. When $\delta = \Omega_0$, the intense LSP is observed but only for a narrow range of ω_p. Moreover, as δ increases further ($\delta = 2\Omega_0$) the range of ω_p to observe intense LSP is narrower. Hence, we conclude that δ depends sensitively on ω_p when δ is larger or comparable to the Ω_0.

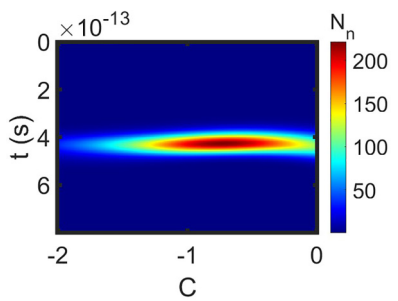

FIG. 9. Temporal profile of N_n at $\delta = \Omega_0$ and $\omega_p = 0.2\Omega_0$.

To encounter the effect of the detuning term, a linearly chirped Gaussian pulse may be used to enhance the LSP. Figure 9 displays the temporal evolution of N_n at $\delta = \Omega_0$ and $\omega_p = 0.2\Omega_0$. Our simulation shows that when $\omega_p < \Omega_0$, a specific chirp is required to obtain the intense N_n; however, as the ω_p reaches closer to or larger than Ω_0, the temporal evolution of N_n remains almost independent of the chirp parameter.

Note that the role of decoherence or dephasing rate is neglected in our simulation. It is well known that the incorporation of decoherence or dephasing will increase the threshold rate and reduce the number of LSPs in the spaser emission [47–50].

IV. CONCLUSION

We have theoretically explored a spaser system that consists of a three-level Λ-type gain medium and a dipolar LSP mode. A Gaussian pulse pumps the QD gain medium. We studied the effects of pulse width, input chirp parameter, and pulse amplitude on the efficiency of LSP generation. We demonstrated that an optimum pulse width and pulse amplitude are required to obtain an intense and Gaussian LSP profile. The pump-pulse energy can be increased by the pulse width or pulse amplitude but that does not always ensure enhancement in LSPs. The temporal profile of a LSP intricately depends on the relative temporal dynamics of the QD gain medium population. In practice, there always exists detuning between the pump-pulse frequency and transition frequency of the gain medium. Therefore, the resonance interaction between a pulse and QDs can occur through ARP phenomena using the linearly chirped pulse. This chirp pump pulse changes the population dynamics of the gain medium, which tunes the temporal and spectral profiles of the LSP. Importantly, for specific values of pulse width, pulse amplitude, and chirp, an intense and Gaussian-shape LSP profile has been demonstrated. Moreover, we also studied the effect of noise, considering the time-harmonic detuning term. It has been shown that when the noise amplitude is near the Rabi constant and the noise frequency is less than the Rabi constant, the pump pulse with the linear chirp can be useful to enhance the number of LSPs. This study is performed with a spherical metal nanoparticle and QDs gain medium, but the model used here can well be employed for explaining other plasmon-based lasing systems [43].

This research underscores the importance of tailoring the pump-pulse parameters to generate robust spaser pulses using semiconductor QDs, which may have diverse applications in

nanoscale data processing, super-resolution imaging, targeted drug delivery, and highly sensitive biosensing, revolutionizing fields such as nanophotonics, medicine, and telecommunications through their unique and compact capabilities.

The data that support the findings of this study are available from the corresponding author upon reasonable request.

ACKNOWLEDGMENT

A.P. expresses sincere gratitude to the University Grants Commission, Government of India, for providing financial support in form of Senior Research Fellowship during his Ph.D.

[1] M. O. Scully and M. Suhail Zubairy, *Quantum Optics* (Cambridge University Press, Cambridge UK, 1999).

[2] C. Cohen-Tannoudji, J. Dupont-Roc, and G. Grynberg, *Atom-Photon Interactions: Basic Processes and Applications* (Wiley, New York, 1998).

[3] N. Passarelli, R. A. Bustos-Marún, and E. A. Coronado, Spaser and optical amplification conditions in gold-coated active nanoparticles, J. Phys. Chem. C **120**, 24941 (2016).

[4] U. Honnester, *Nano and Quantum Optics* (Springer, Cham, 2019).

[5] L. Novotny and B. Hecht, *Principles of Nano-Optics* (Cambridge University Press, Cambridge, UK, 2012).

[6] C.-Z. Ning, Semiconductor nanolasers and the size-energy-efficiency challenge: a review, Adv. Photonics **1**, 014002 (2019).

[7] E.-P. Li and H.-S. Chu, *Plasmonic Nanoelectronics and Sensing* (Cambridge University Press, Cambridge, UK, 2014).

[8] L. Prelat, N. Passarelli, R. Bustos-Marún, and R. A. Depine, Terahertz lasing conditions of radiative and nonradiative propagating plasmon modes in graphene-coated cylinders, J. Opt. Soc. Am. B **39**, 2547 (2022).

[9] M. I. Stockman, Nanoplasmonics: Past, present, and glimpse into future, Opt. Express **19**, 22029 (2011).

[10] P. Törmä and W. L. Barnes, Strong coupling between surface plasmon polaritons and emitters: a review, Rep. Prog. Phys. **78**, 013901 (2014).

[11] O. Bitton, S. Nath Gupta, and G. Haran, Quantum dot plasmonics: From weak to strong coupling, Nanophotonics **8**, 559 (2019).

[12] R.-M. Ma and R. F. Oulton, Applications of nanolasers, Nat. Nanotechnol. **14**, 12 (2019).

[13] L. Prelat, M. Cuevas, N. Passarelli, R. B. Marún, and Ricardo Depine, Spaser and optical amplification conditions in graphene-coated active wires, J. Opt. Soc. Am. B **38**, 2118 (2021).

[14] P. K. Jha, Y. Wang, X. Ren, and X. Zhang, Quantum-coherence-enhanced transient surface plasmon lasing, J. Opt. **19**, 054002 (2017).

[15] S. Gwo and C.-K. Shih, Semiconductor plasmonic nanolasers: Current status and perspectives, Rep. Prog. Phys. **79**, 086501 (2016).

[16] D. J. Bergman and M. I. Stockman, Surface plasmon amplification by stimulated emission of radiation: Quantum generation of coherent surface plasmons in nanosystems, Phys. Rev. Lett. **90**, 027402 (2003).

[17] M. I. Stockman and D. J. Bergman, Method for surface plasmon amplification by stimulated emission of radiation (SPASER), U.S. Patent No. US8017406B2 (2011).

[18] M. T. Hill, Y.-S. Oei, B. Smalbrugge, Y. Zhu, T. de Vries, P. J. van Veldhoven, F. W. M. van Otten, T. J. Eijkemans, J. P. Turkiewicz, H. de Waardt *et al.*, Lasing in metallic-coated nanocavities, Nat. Photon. **1**, 589 (2007).

[19] R. F. Oulton, V. J. Sorger, T. Zentgraf, R.-M. Ma, C. Gladden, L. Dai, G. Bartal, and X. Zhang, Plasmon lasers at deep subwavelength scale, Nature (London) **461**, 629 (2009).

[20] K. Yu, A. Lakhani, and M. C. Wu, Subwavelength metal-optic semiconductor nanopatch lasers, Opt. Express **18**, 8790 (2010).

[21] S.-H. Kwon, J.-H. Kang, C. Seassal, S.-K. Kim, P. Regreny, Y.-H. Lee, C. M. Lieber, and H.-G. Park, Subwavelength plasmonic lasing from a semiconductor nanodisk with silver nanopan cavity, Nano Lett. **10**, 3679 (2010).

[22] E. I. Galanzha, R. Weingold, D. A. Nedosekin, M. Sarimollaoglu, J. Nolan, W. Harrington, A. S. Kuchyanov, R. G. Parkhomenko, F. Watanabe, Z. Nima *et al.*, Spaser as a biological probe, Nat. Commun. **8**, 15528 (2017).

[23] X.-Y. Wang, Y.-L. Wang, S. Wang, B. Li, X.-W. Zhang, L. Dai, and R.-M. Ma, Lasing enhanced surface plasmon resonance sensing, Nanophotonics **6**, 472 (2017).

[24] R.-M. Ma, X. Yin, R. F. Oulton, V. J. Sorger, and X. Zhang, Multiplexed and electrically modulated plasmon laser circuit, Nano Lett. **12**, 5396 (2012).

[25] C. Zhang, Y. Lu, Y. Ni, M. Li, L. Mao, C. Liu, D. Zhang, H. Ming, and P. Wang, Plasmonic lasing of nanocavity embedding in metallic nanoantenna array, Nano Lett. **15**, 1382 (2015).

[26] P.-J. Cheng, Z.-T. Huang, J.-H. Li, B.-T. Chou, Y.-H. Chou, W.-C. Lo, K.-P. Chen, T.-C. Lu, and T.-R. Lin, High-performance plasmonic nanolasers with a nanotrench defect cavity for sensing applications, ACS Photonics **5**, 2638 (2018).

[27] A. Purohit and A. K. Mishra, A comparative study of coherent and incoherent drives in a four-level quantum dot–based spaser, J. Opt. **26**, 035001 (2024).

[28] A. Purohit, V. S. Poonia, and A. K. Mishra, Effect of electron phonon interactions on three-level QD-based spaser: Linear and quadratic potentials, J. Opt. **26**, 045201 (2024).

[29] M. O. Sargent, M. O. Scully, and W. E. J. Lamb, *Laser Physics* (Addison-Wesley, Reading, MA, 1977).

[30] W. S. Warren, J. L. Bates, M. A. McCoy, M. Navratil, and L. Mueller, There were no pi pulses in iodine vapor: Crafted pulses to compensate for Rabi-frequency inhomogeneities, J. Opt. Soc. Am. B **3**, 488 (1986).

[31] V. S. Malinovsky and J. L. Krause, General theory of population transfer by adiabatic rapid passage with intense, chirped laser pulses, Eur. Phys. J. D **14**, 147 (2001).

[32] J. S. Melinger, S. R. Gandhi, A. Hariharan, D. Goswami, and W. S. Warren, Adiabatic population transfer with frequency-swept laser pulses, J. Chem. Phys. **101**, 6439 (1994).

[33] J. S. Melinger, S. R. Gandhi, A. Hariharan, J. X. Tull, and W. S. Warren, Generation of narrowband inversion with broadband laser pulses, Phys. Rev. Lett. **68**, 2000 (1992).

[34] H. Maeda, J. H. Gurian, D. V. L. Norum, and T. F. Gallagher, Coherent population transfer in an atom by multiphoton adiabatic rapid passage, Phys. Rev. Lett. **96**, 073002 (2006).

[35] G. P. Agrawal, Nonlinear fiber optics, in *Nonlinear Science at the Dawn of the 21st Century*, Lecture Notes in Physics, edited by P. L. Christiansen, M. P. Sørensen, and A. C. Scott (Springer, Berlin, Heidelberg, 2000), pp. 195–211.

[36] R. Trebino, *Frequency-Resolved Optical Gating: The Measurement of Ultrashort Laser Pulses* (Springer Science & Business Media, New York, 2000).

[37] A. K. Mishra, O. Karni, and G. Eisenstein, Coherent control in quantum dot gain media using shaped pulses: A numerical study, Opt. Express **23**, 29940 (2015).

[38] O. Karni, A. Kumar Mishra, G. Eisenstein, V. Ivanov, and J. P. Reithmaier, Coherent control in room-temperature quantum dot semiconductor optical amplifiers using shaped pulses, Optica **3**, 570 (2016).

[39] K. Li, D. C. Spierings, and A. M. Steinberg, Efficient adiabatic rapid passage in the presence of noise, Phys. Rev. A **108**, 012615 (2023).

[40] K. M. Weiss, J. M. Elzerman, Y. L. Delley, J. Miguel-Sanchez, and A. Imamoğlu, Coherent two-electron spin qubits in an optically active pair of coupled InGaAs quantum dots, Phys. Rev. Lett. **109**, 107401 (2012).

[41] D. Brunner, B. D. Gerardot, P. A. Dalgarno, G. Wüst, K. Karrai, N. G. Stoltz, P. M. Petroff, and R. J. Warburton, A coherent single-hole spin in a semiconductor, Science **325**, 70 (2009).

[42] D. Zhao, Y. Gu, J. Wu, J. Zhang, T. Zhang, B. D. Gerardot, and Q. Gong, Quantum-dot gain without inversion: Effects of dark plasmon-exciton hybridization, Phys. Rev. B **89**, 245433 (2014).

[43] M. M. Tohari and M. M. Alqahtani, Gain without population inversion and superluminal propagation in the metal nanoparticles-graphene nanodisks-quantum dots hybrid systems, J. Phys.: Condens. Matter **33**, 325302 (2021).

[44] J. D. Cox, M. R. Singh, G. Gumbs, M. A. Anton, and F. Carreno, Dipole-dipole interaction between a quantum dot and a graphene nanodisk, Phys. Rev. B **86**, 125452 (2012).

[45] H. Rose, O. V. Tikhonova, T. Meier, and P. R. Sharapova, Steady states of Λ-type three-level systems excited by quantum light with various photon statistics in lossy cavities, New J. Phys. **24**, 063020 (2022).

[46] N. Chanda, P. Patnaik, and R. Bhattacharyya, Optimal population transfer using adiabatic rapid passage in the presence of drive-induced dissipation, Phys. Rev. A **107**, 063708 (2023).

[47] D. J. Trivedi, D. Wang, T. W. Odom, and G. C. Schatz, Model for describing plasmonic nanolasers using Maxwell-Liouville equations with finite-difference time-domain calculations, Phys. Rev. A **96**, 053825 (2017).

[48] K. E. Dorfman, P. K. Jha, D. V. Voronine, P. Genevet, F. Capasso, and M. O. Scully, Quantum-coherence-enhanced surface plasmon amplification by stimulated emission of radiation, Phys. Rev. Lett. **111**, 043601 (2013).

[49] P. Zhang, I. Protsenko, V. Sandoghdar, and X.-W. Chen, A single-emitter gain medium for bright coherent radiation from a plasmonic nanoresonator, ACS Photonics **4**, 2738 (2017).

[50] P. Song, J.-H. Wang, M. Zhang, F. Yang, H.-J. Lu, B. Kang, J.-J. Xu, and H.-Y. Chen, Three-level spaser for next-generation luminescent nanoprobe, Sci. Adv. **4**, eaat0292 (2018).